Developing A Diffraction Pattern Projection System for Neutral Atom Quantum Computation

A Senior Project

presented to

the Faculty of the Physics Department

California Polytechnic State University, San Luis Obispo

In Partial Fulfillment

of the Requirements for the Degree

Bachelor of Science

by

Sanjay Khatri

March, 2014

TABLE OF CONTENTS

LIST OF TABLES

LIST OF FIGURES

1. Introduction

1.1 Motivation for Pursuing Quantum Computation

As manufacturers develop smaller chips, quantum mechanical effects will begin to dominate, and thus the chip will not perform as expected, classically. With technological pushes toward smaller electronic devices, the chips must account for quantum mechanics to perform computations as opposed to the classical physics techniques [1]. This movement suggests that we incorporate a different paradigm for performing certain computations. Furthermore, attempts to create smaller chips for different applications have fueled current interest in quantum computation. Instead of classical bits, "qubits" or quantum bits are incorporated inside the chips, which now obey quantum mechanics. The main distinction between these types of computers is that the qubits can be in a superposition of states,

$$\psi = a|0\rangle + b|1\rangle, \tag{1}$$

where a, b are the respective probability amplitudes for the states $|0\rangle$ and $|1\rangle$. The superposition of states reduces the overall number of operations to arrive at the desired output. However, a direct measurement of the system collapses the measurement to only one of the qubit's states. Therefore, several measurements of the system are required in order to determine the state of the qubit.

Chip manufacturers must account for quantum mechanical effects, which can drastically alter the behavior of the system if not accounted for. Despite these complications, quantum computations are able to perform some operations more efficiently compared to classical computers. Efficiency is defined as the minimal steps required in performing a specific operation. Shor's Algorithm, for example, can factor very large numbers exponentially faster than a classical computer to arrive at the result. It would be impossible for classical computers to be able to compute the prime factorization of very large numbers within a time frame extending to the age of the universe, but a quantum computer can determine the number's factorization well within a reasonable time frame. There are several options for selecting a system to use as a qubit, but we are working towards utilizing neutral atoms for quantum computation.

1.2 Using Neutral Atoms for Quantum Computation

The focus of our efforts is to develop a system for neutral atom quantum computation. In neutral atom quantum computing, the goal is to perform quantum algorithms with certain states of neutral atoms serving as qubits. Trapping neutral atoms is a vital step toward being able to implement quantum algorithms. However, a neutral atom quantum computer must have five qualities according to DiVincenzo [2]. A quantum system must contain approximately 10^6 qubits that are comprised of at least two states representing 0 and 1. We must be able to initialize the state of the entire system to a known state. We can change the state of the system by being able to perform a set of quantum gates, which includes single- and two-qubit gates. The qubit states must be stable and possess long lifetimes, thereby reducing decoherence. Decoherence occurs when the phases for the basis states begin to evolve randomly due to the system's coupling with the environment [2]. Finally, we must be able to read the qubit state. Keeping these criteria in mind, our current efforts are geared toward preparing a large addressable array of qubits.

For the purposes of our experiment, we will use alkali atoms for neutral atom quantum computation. Alkali atoms have only one valence electron with two hyperfine ground states. The two hyperfine ground states will be used as qubit states, since the ground states have long lifetimes, thus reducing decoherence of the system. Therefore, neutral atoms have weaker coupling to the environment and are less responsive to extraneous electromagnetic fields than ions, for example.

Trapping atoms is a crucial first step towards performing quantum algorithms. In order to trap the atoms, they must first be placed in an Ultra-High Vacuum (UHV) setting, which minimizes the perturbations of the atoms by other gases. With the atoms in an UHV environment, we cool the atoms using a magneto-optical trap (MOT). The MOT will significantly reduce the velocity of the atoms and have them congregate at the center of the MOT. Once cooled, we can transfer the atoms from the MOT to a light trap, which will use only laser light to trap atoms. With the

MOT cooling the atoms to about $200\ \mu K$, projecting the 1 mK pinhole pattern into the center of the MOT should trap the atoms.

2. Experimental Methods for Cooling and Trapping Neutral Atoms

2.1 Magneto Optical Trap (MOT)

The initial cooling of the ^{87}Rb atoms in the UHV chamber is performed using a magneto-optical trap (MOT). The atoms in the chamber travel in all directions and we must devise a method for slowing them down regardless of the direction the atoms travel. To do so, we will be using Doppler cooling, which exploits the Doppler Effect to cool the atoms. For the MOT, we will be using two laser beams for each translation degree of freedom for the atoms, which amounts to six total laser beams. The lasers will be detuned to the "red" (at a lower frequency) of the transition. Atoms travelling toward one laser will experience a higher frequency due to the Doppler Effect, thus being closer to resonance. As a result, the atoms travelling toward the laser will absorb more photons. Atoms traveling away from the laser will observe a lower frequency, which would make the laser's frequency further from resonance. As a result, the laser photons travelling in the direction of the atom will be absorbed less, while photons travelling against the atom will be absorbed more often creating a net effect of decreasing the atom's kinetic energy.

In our setup, we use 780 nm laser light tuned to the transition energy of ^{87}Rb . Two lasers are needed to accomplish laser cooling of the atoms. One laser beam excites the electrons from (F=2) to the (F=3) state represented by the black line in Figure 2.1. From this excited state, quantum mechanical selection rules only allow the electron to drop back down to the F=2 ground state, where it can once again absorb another photon. This transition is therefore known as the cycling transition. The excited state has a lifetime of has a 26.9 nanosecond meaning that the cycle repeats several times per second. Because the momentum kick for each is in the direction of the laser photon and the subsequent spontaneous emissions occur randomly in all directions, the atom receives an overall change in momentum in the direction of the laser beam. However, sometimes the electron may fall back into another hyperfine ground state (F=1) via other processes. With our laser tuned to the F=2 to F=3 transition, the atoms in the F=1 state will not be excited, so we included a second laser known as the pump laser, which is represented as the

dashed red line in Figure 2.1. The pump laser is used to re-excite the electrons that have de-excited to the F=1 state back to the (F = 2) excited state. This will ensure that the cycling transition and thus the cooling can continue.

Doppler cooling decreases the kinetic energy of the atoms, but reducing the energy will only cool the atoms, but we also want to collect as many cold atoms at the center trap.

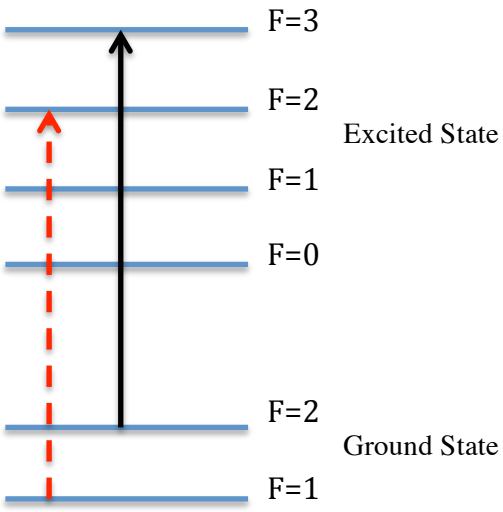

Figure 2.1 Electron D_2 transition required for cooling ^{87}Rb . The dash line represents a pump laser to excite the atoms in the F=1 ground state and have it return to the F=2 ground state. The solid black line represents the other laser exciting the atom from the F=2 ground state to the F = 3 excited state.

In order to collect atoms at the center of the chamber, we create a magnetic quadrupole field in the chamber using an Anti-Helmholtz coil configuration as shown in Fig. 2.2.

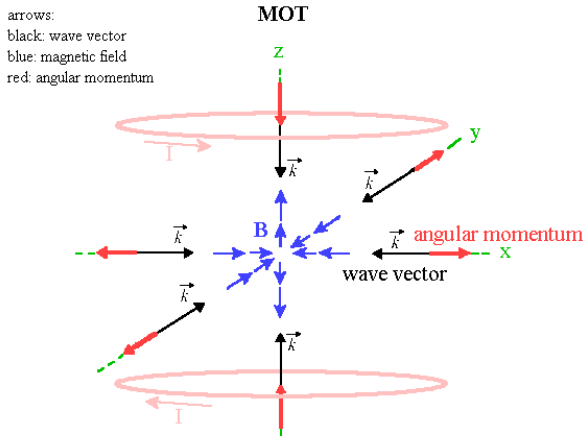

Figure 2.2 Anti-Helmholtz coil configuration used for the magneto-optical trap. [3]

The two pink rings represent the wires from the magnetic coils, where the current flow in opposite directions generates a quadrupole magnetic field, **B**, that is zero at the center of the coils and increases linearly in all directions near the center as shown in Fig. 2.3.

The σ_+ and σ_- symbols in Fig. 2.3 refer to the angular momentum polarization of the laser beams travelling in the positive and negative z-direction, respectively. The circular polarization of the lasers can be created from the linearly polarized diode laser output and using a quarter wave-plate. It is crucial for these lasers to be polarized correctly, in order for the atoms to receive numerous momentum kicks toward the center of the trap but rarely away from it.

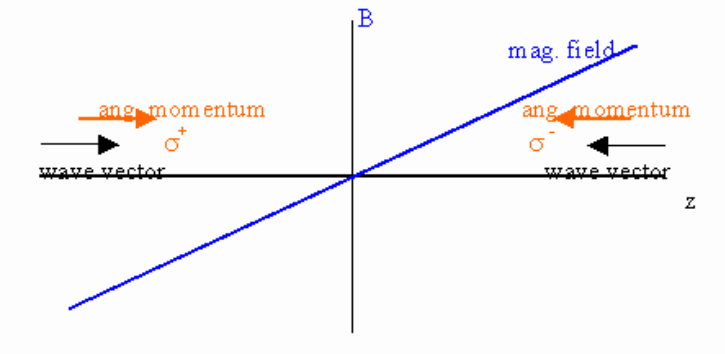

Figure 2.3 Magnetic field (B) near the center of the coils as a function of position (z). The arrows represent the circularly polarized lasers (σ_+ from the left and σ_- from the right). [3]

We determined the effect that the external magnetic field has on the energy levels of the atom using Fig. 2.3 and the equation,

$$U = -\boldsymbol{\mu} \cdot \boldsymbol{B}, \tag{2}$$

where $\boldsymbol{\mu}$ is the magnetic dipole moment and $\boldsymbol{B}$ is the magnetic field. We can re-write equation 2 as,

$$U = g m_F \mu_B B_z, \tag{3}$$

where g is the Lande g-factor, m_F is the magnetic quantum number associated with the total angular momentum, μ_B is the Bohr magneton, and B_z is the z-component of the magnetic field.

To explain how the effect of the magnetic field leads to trapping, consider a simplified atom. Figure 2.4 shows the three magnetic substates ($m_J = 0, \pm 1$) of the J = 1 state when the atom is placed into the magnetic quadrupole field.

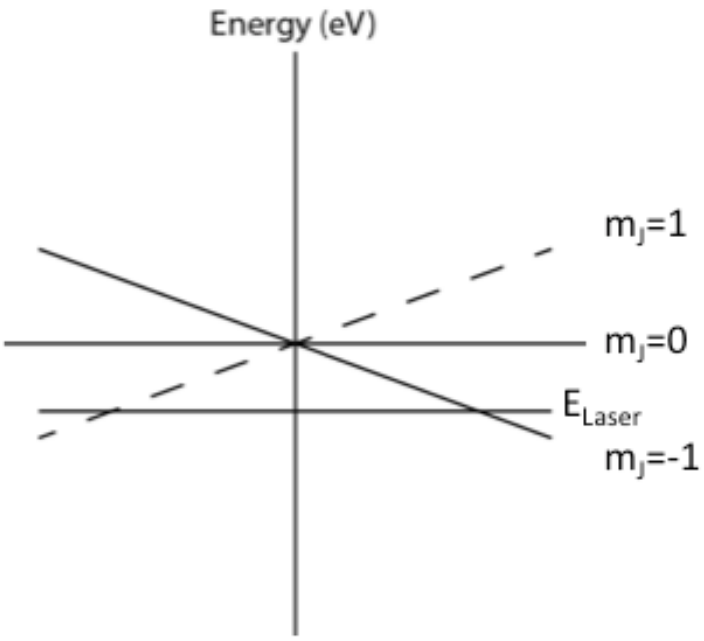

Figure 2.4 Zeeman Splitting of the excited state energy level due to the external magnetic field (ground state not shown). The green and pink lines represent the $m_J = \pm 1$ respective magnetic sub-states of a simplified atom with the ground state J=0 and a J=1 excited state. The black horizontal line indicates the energy of the laser. [3]

The J=0 ground state (not shown) would be below the three energy states shown in Fig 2.4. This atomic energy level splitting due to an external magnetic field is known as the Zeeman Effect. As indicated in Fig. 2.3, a σ_+ polarized laser beam comes from the left, and σ_- polarized laser beam comes from the right. Consider an atom left of the center of the MOT cell (z<0), then our goal is to move the atom as close to the center (z=0) as possible. According to Fig. 2.4, the σ_+ laser is in resonance with the atom, as the energy of the laser is closer to the $m_J = 1$ state than the $m_J = -1$ state. There may still be some σ_- absorbed in the region (z>0), but it is not as frequent as σ_+ absorption. As a result, the net force will direct the atom toward the center of the chamber. Conversely, for an atom located to the right of the center (z>0), the σ_- polarized laser beam is in resonance with the atom, where the laser's energy is closer to $m_J = -1$ than $m_J = 1$. In contrast with the σ_+ laser, the majority of the photons from the σ_-laser will be absorbed by the

atom compared to the lower probability of absorption from the σ_+ laser. With the σ_- laser pointed toward the center, the net force exerted on the atom will also be toward the center of the chamber (z=0).

In this technique, atoms will always be directed toward the center, but never away from it. The atoms are thus trapped at the center. The MOT cools atoms from room temperature to about $200\ \mu K$ and collects them in a cloud at the center of the trap, which is the first step in any cooling and trapping experiment.

2.2 Atomic Dipole Trapping in the Diffraction Pattern Behind A Pinhole

The next portion of the experiment involves transferring the atoms from the MOT to the light traps. With the MOT lasers and magnetic field switched off, we then expose the cold neutral ^{87}Rb atoms to the light trap lasers. Lasers are electromagnetic waves composed of an oscillating electric and magnetic field. The polarization of the electric field will induce an electric dipole onto the neutral atom. The dipole experiences a force due to the electric field of the laser, which is known as the optical dipole force. We will exploit the optical dipole force by confining cold neutral atoms within a varied laser intensity field. The atoms will reside in areas of minimizing their potential energy. Depending on the laser's frequency, the dipoles will be attracted toward areas of higher or lower intensity, which correspond to the respective bright or dark spots. A red detuned trap (RDT) forms when the laser's frequency is tuned below the resonance frequency of the atomic transition. The trap location of a RDT is at an intensity maximum, which is the location of minimum dipole potential energy. The minimum dipole potential energy with a blue detuned trap (BDT) occurs at intensity minima. Creating these bright (RDT) and dark (BDT) spot patterns will enable us to trap neutral atoms.

For the purposes of this experiment, we will create localized bright and dark spot traps using the diffracted light formed behind a circular aperture to trap neutral atoms [4]. The varied intensity distributions create perfect regions for either RDTs or BDTs. We will attempt to implement both traps, but we are currently interested in the blue-detuned traps, since dark regions of the pattern can create longer and stable trap lifetimes. Creating the diffraction pattern inside the MOT would require the aperture to be included with the design and construction of the vacuum chamber as

well as the optical system desired for cooling the atoms. The entire optical system would have to be implemented inside the chamber, which could cause several experimental challenges. To avoid these experimental technicalities, we will project the pattern into the MOT [5] as shown in Fig. 2.5.

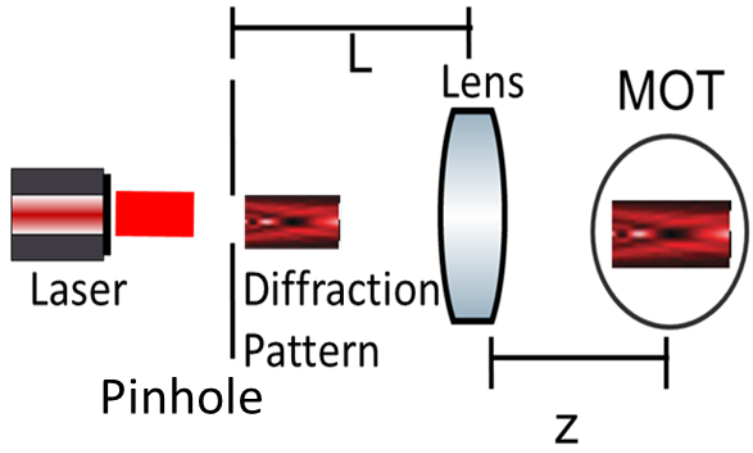

Figure 2.5 Experimental pinhole diffraction system.

We modeled the diffraction pattern directly behind a pinhole using Hertz Vector Diffraction Theory (HVDT) to determine the electric field just beyond the aperture. We assume that plane waves from the laser initially pass through the pinhole, meaning that the electric field has a constant amplitude and phase of oscillation across the aperture. After the light passes through the pinhole, diffraction effects create areas of bright and dark spots directly behind the pinhole. In HVDT, we integrate the electric field along the aperture to determine the field directly behind the pinhole. Since we will use a lens placed further away from the pinhole, we can model the electric field using Fresnel Diffraction. For points of interest a distance larger than the aperture radius, a, the intensity is cylindrically symmetric [5].

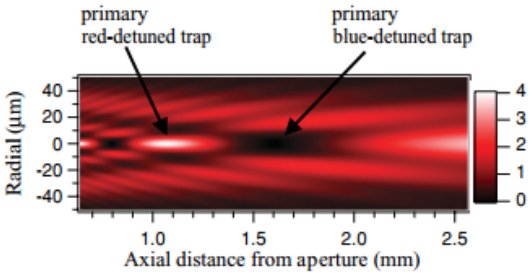

Figure 2.6 Diffraction pattern formed directly behind a pinhole.

The electric field beyond the pinhole in the Fresnel diffraction regime is [5],

$$E_1(r_1, z_1) = \frac{ke^{ikz_1}}{iz_1} e^{\left[i\frac{kr_1^2}{2z_1}\right]} \times \int_0^a E_{z_0} J_0\left(\frac{kr_0 r_1}{z_1}\right) e^{i\frac{kr_0^2}{2z_1}} r_0 dr_0, \tag{4}$$

where r_1, z_1 are the coordinates for the point of interest, k is the wave number, r_0 is the integration point in the aperture plane, and E_{z_0} is the incident z-component of the electric field. J_0 is the Bessel function of the first kind of order zero. The effect of the lens on the wave can be accounted for with the thin lens transformation, $t(r_L)$. We can relate the electric field leaving the lens with the field incident on the lens by [5]

$$E_L(r_L, z_L = 0) = E_1(r_1, z_1 = L) t(r_L), \tag{5}$$

where E_L is the electric field exiting the lens, E_1 is the electric field incident upon the lens, and $t(r_L)$ is the thin lens phase transformation as a function of the radial distance from the optical axis. The final result of the electric field projected at the center of the MOT cloud is given by [5],

$$E(r, z) = \frac{dke^{ik(z+L)}}{iLz} e^{i\frac{k}{2z}\left(1-\frac{d}{z}\right)r^2} \times \int_0^a E_{z_0} J_0\left(\frac{kr_0 rd}{Lz}\right) \times e^{\left[i\frac{k}{2L}\left(1-\frac{d}{L}\right)r_0^2\right]} r_0 dr_0, \tag{6}$$

where $d = \left[\frac{1}{L} + \frac{1}{z} - \frac{1}{f}\right]^{-1}$, z is the distance between the lens and the center of the MOT, L is the distance between the pinhole and the lens, and f is the focal length of the lens. The integration will allow us to map the electric field distribution at the center of the MOT cloud.

To determine the location of the projected bright and dark spots on the optical axis, we set $r = 0$ in equation 6, where we can extract their locations given by [5],

$$z = f \frac{1 - nL\frac{\lambda}{a^2}}{1 - n(L - f)\frac{\lambda}{a^2}}, \tag{7}$$

where λ is the wavelength of the laser beam, a is the radius of the pinhole, f is the focal length of the lens, and n is the trap index. The trap index is an integer value ascribed to each bright or

dark spot trap starting with the one furthest from the aperture. Since we are primarily interested in the primary dark spot trap, the trap index (n) would be 2. The primary dark spot trap is blue-detuned, which is the dark spot furthest from the aperture as shown in Fig. 2.6.

The main focus of this experiment was to construct the optical setup for the projected system and ensure it was aligned with respect to the center of MOT. The next section covers the required steps for creating the projection system, aligning the system to match the height of the center of the MOT, and determining the location for each trap site.

3. Atomic Dipole Trapping Pattern Results

3.1 Construction of the Optical System for Projecting the Diffraction Pattern

In our particular experimental setup, we will use a lens with a focal length $f = 75\ mm$ to project the pattern into the MOT. Alignment of the projection system is absolutely crucial, so that the pattern can be projected as close to the center of the MOT cloud as possible. Thus, we placed the pinhole with a radius $a = 50\ \mu m$ and the projection lens on a cage system [7]. The cage system as shown in Fig. 3.1 facilitated the laser alignment process and also allowed for quick alteration of the distance between the pinhole and the lens.

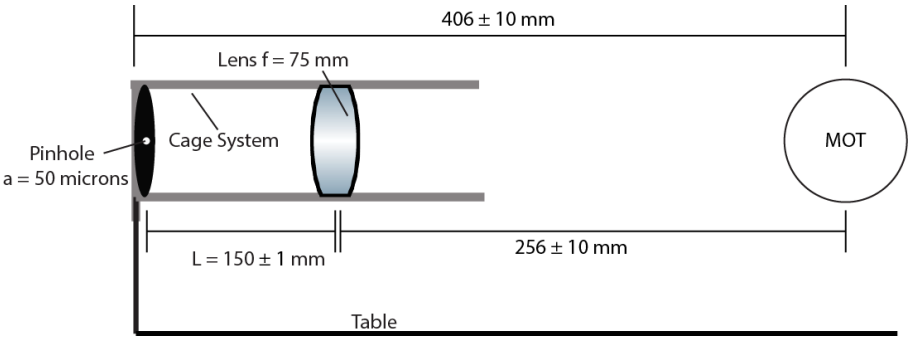

Figure 3.1 Experimental optical system for projecting the diffraction pattern into the center of the MOT.

A picture of the experimental setup is shown in Fig. 3.2.

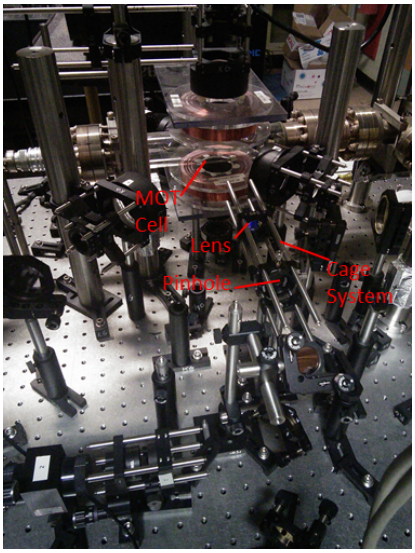

Figure 3.2 Picture of experimental setup for projecting the diffraction pattern into the MOT cell.

Adjusting the position of the lens with respect to the pinhole will project the localized bright and dark spot pattern at a specific distance from the lens. To preserve the size and shape of the projected pattern, the distance between the pinhole and the lens, L, should approximately be $2f$, where f is the focal length of the lens. For a given lens with focal length f, variation in the distance between the lens and pinhole (L) results in different pattern sizes. Table 3.1 summarizes all of the possible scenarios for relating L and the size of the projected pattern.

$L < 2f$	Image is magnified
$L > 2f$	Image is reduced in size
$L = 2f$	Image is same size as original pattern

Table 3.1 Relationship of the image size to the relative sizes of L and f.

With the cage system built, we now need to set the height of the pinhole to the height of the MOT's center.

3.2 Measuring the height of the center of the MOT

The next major challenge was determining the height of the cage system and its orientation along the z-axis, with the axis shown in Fig 2.3. For orienting the system along the z-axis, the holes on the optical table were a fairly reliable approximation for estimating the center of MOT.

Previously, alignment was performed so that the laser beams entering from below the vacuum chamber z-axis were aligned along the same pattern of holes on the table.

Measuring the height of the MOT required taking careful measurements using calipers with a $0.1\ mm$ resolution. Averaging the distance between the bottom of the higher magnetic coil and the top of the lower magnetic coil provided a close approximation of the center of the MOT as shown in Fig. 3.3. The spacing between the coils was measured to be $60\ mm$, so the location of the center between the two coils would be $30\ mm$ above the bottom coil.

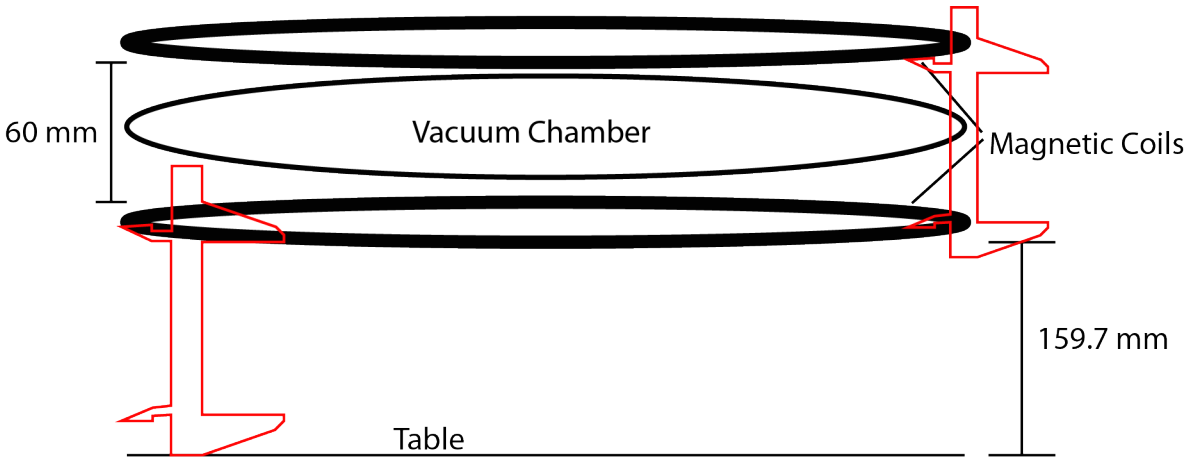

Figure 3.3 Schematic for measuring the center of the MOT. Orientation of the calipers is shown in red.

The height from the table to the top of the lower magnetic coil was 159.7 mm as shown in Fig. 3.3. Summing the two results yields that the center of the MOT was measured to be $189.7\ mm$ above the table. A picture of the specific locations for each measurement is depicted in Fig. 3.4.

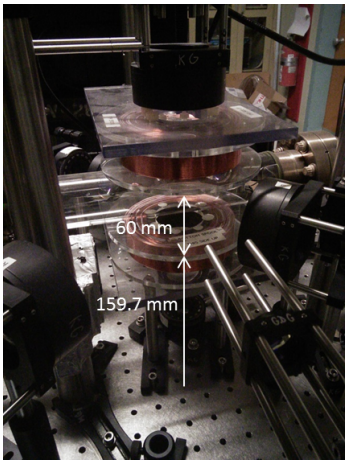

Figure 3.4 Picture of the locations for each height measurement in determining the center of the MOT.

When using the calipers, it was crucial to ensure the reading from the calipers matched the actual distance it measured. When measuring the distance from the table to the lower magnetic coil, the calipers displayed the reading but excluded the 14.2 mm bias based on the orientation required to make the measurement as shown in Fig. 3.3. The bias was added to the value recorded by the calipers as shown in Fig. 3.5.

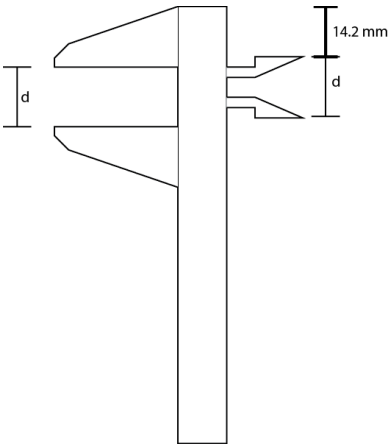

Figure 3.5 Calipers schematic including the additional bias of 14.2 mm when measuring the height of the MOT's center

After measuring the position of the MOT's center, we had to adjust the height of the cage system to ensure the height of the incident laser beam was at 189.7 mm. When measuring the height of the laser beam, we used a t-shirt target that contained a line along the center of the cage system. To ensure that line was 189.7 mm above the table, we placed a post inside a post holder (Thorlabs PH2) with a flat base (Thorlabs BA1S) connected to the top of the post as shown in Fig. 3.6.

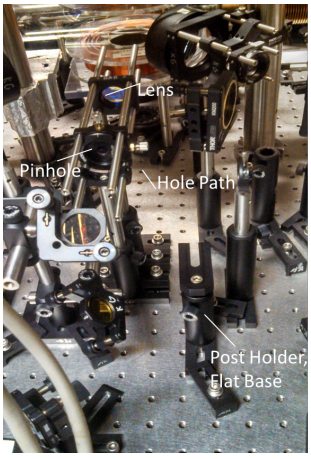

Figure 3.6 Experimental setup for measuring the height of the pinhole.

We placed it near the cage system so that the calipers had a stable base for measuring the height of the center of the cage system as accurately as possible. The heights for the post holder (PH2), and the two bases (BA1, BA1S) as well as the entire measurement system are shown in Fig. 3.7. We verified the dimensions posted on the actual parts with the calipers. Knowing the height of each element, we added the known heights plus the reading on the calipers to accurately set the center of the cage system to be $189.7mm$.

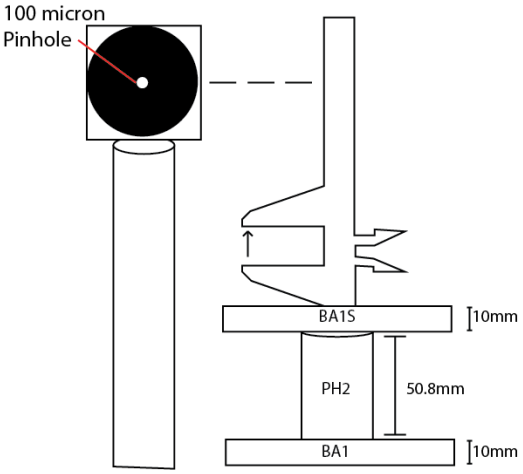

Figure 3.7 Measurement system for setting the height of the pinhole to be 189.7 mm.

3.3 Experimental Test Setup for Viewing Trap Sites

With our projection system constructed, the next step was to view the different locations of the primary bright and dark spot trap sites. We placed the system on optical rails and used a Thorlabs DCC1645C CMOS camera to monitor the diffraction pattern as shown in Figures 3.8 and 3.9. The optical rails allowed us to easily adjust the position of the camera relative to the projection system without altering the lateral position, so it was possible for us to view the trapping patterns and record their respective locations from the projection lens. To be able to view the trap locations, we set the aperture to lens distance (L) to be $114 \pm 1\ mm$. Setting $L < 2f$ caused the image of the pattern to be magnified in size, so we could view the pattern with the camera, which has a pixel size of $5.2\ \mu m$.

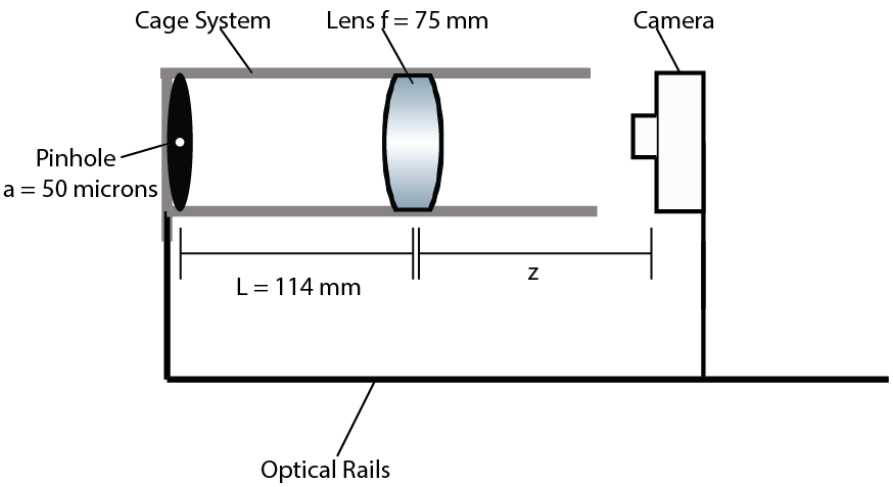

Figure 3.8 an optical rail system for determining the locations of the trap sites.

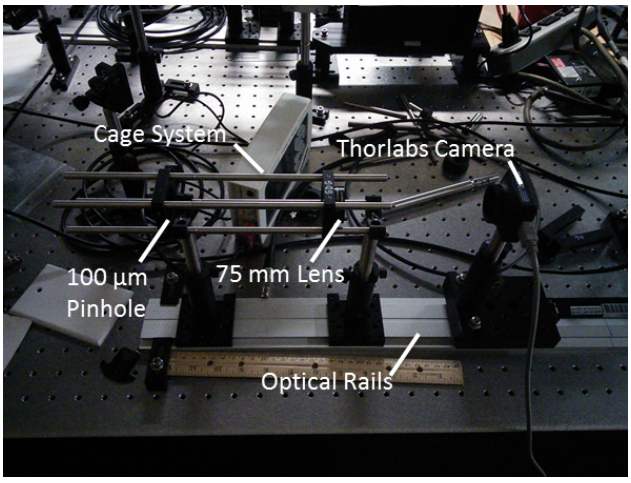

Figure 3.9 Photograph of the optical rail system.

By sliding the camera, we were able to view the different bright and dark spot trap sites. Figures 3.10 and 3.11 depict the first four trap sites. With the given parameters: $L = 114\,mm,\ a = 50\,\mu m,\ f = 75\,mm$, and $\lambda = 780\,nm,$ we measured and then computed the theoretical values of the distance from the lens to the location of each trap site (z) as predicted by equation 1. A standard 12-inch ruler was used to measure the distance between the projection lens and the location for each trap site.

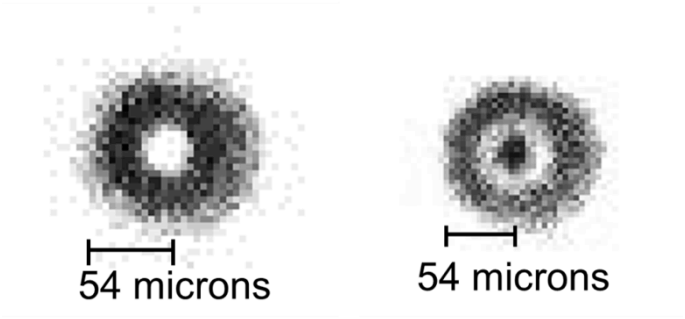

Figure 3.10 Bright (n=1) and dark (n=2) spot trap patterns. $L = 114 \pm 1\ mm$, $a = 50\ \mu m$, $f = 75\ mm$, and $\lambda = 780\ nm$.

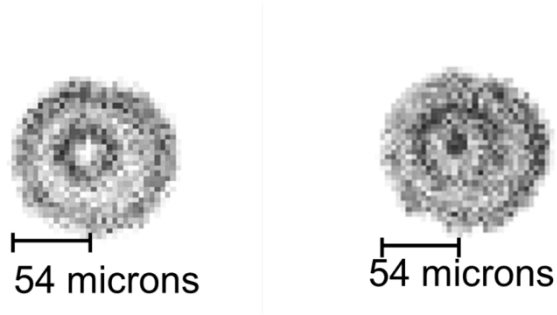

Figure 3.11 Bright (n=3) and dark (n=4) spot trap patterns. $L = 114 \pm 1\ mm$, $a = 50\ \mu m$, $f = 75\ mm$, and $\lambda = 780\ nm$.

Trap Index (n)	Experimental Result (cm)	Theoretical Value (cm)
1	22.5 ± 0.1	23.2 ± 0.4
2	22.3 ± 0.1	22.5 ± 0.4
3	22.0 ± 0.1	22.3 ± 0.4
4	21.9 ± 0.1	22.2 ± 0.4

Table 3.2 Experimental vs Theoretical values for the distance between the lens and each trap site.

Knowing that the pixel distance for the Thorlabs camera was $5.2\ \mu m$, we determined the width of each pattern as shown in Figures 3.10 and 3.11. The trap sites in Fig. 3.10 contain larger trapping regions compared to that of the traps in Fig. 3.11.

Based on our results in Table 3.2, the location of the experimental primary bright (n=3) and dark spot (n=2) trap site calculations were within the uncertainty of the theoretical calculations. With our current interest in the primary dark spot for our light traps, we were pleased that the experimental z-value was within the uncertainty of the theoretical calculation. However, since the uncertainty extends beyond the dimensions of the MOT cloud, approximately $2\ mm$ in size, we would need to implement an alternative method for conducting these measurements with a

smaller uncertainty. We could use a translation stage with a fine micrometer when recording the z-measurements to further reduce uncertainty to within the dimensions of the MOT cloud. This will then enable us to determine whether the projected pattern falls within the dimensions of the MOT cloud. We want to eventually use the measured z-values for the trap sites and incorporate them in our original set up in section 3.1 for projecting the pattern into the center of the MOT cloud.

4. Conclusions

We are exploring a possible solution to the scalability problem of neutral atom quantum computing. Our proposed solution includes using light traps formed in the diffraction pattern directly behind a pinhole as a possible basis for a quantum memory. We designed and set up an optical system for projecting the diffraction pattern into our MOT cloud. Projecting the pattern into the MOT eliminates numerous technical difficulties associated with placing the diffraction aperture within the vacuum chamber. We carefully measured the location of the MOT's center and the locations of the trap sites in the projected diffraction pattern. Although our experimental trap site locations were within the uncertainty of the theoretical values, the uncertainty extends beyond the dimensions of the MOT cloud. Ultimately, we expect to transfer the atoms into the projected light traps and measure their properties to determine whether they are indeed viable for quantum computing.

5. Bibliography

1. Nielsen, Michael A., and Isaac L. Chuang. *Quantum computation and quantum information*. Cambridge university press, 2010.
2. DiVincenzo, D.P., The Physical Implementation of Quantum Computation. Fortschritte der Physik, (2000).
3. Magneto-optical Trap." *Jkrieger.de/ MOT*. N.p., n.d. Web. 31 May 2013.
4. G. D. Gillen, S. Guha, and K. Christandl, Phys. Rev. A 73, 013409 (2006).
5. K. Gillen-Christandl and G. D. Gillen, Phys. Rev. A 82, 063420 (2010)
6. Pedrotti, Frank L., Leno S. Pedrotti, and Leno S. Pedrotti. *Introduction to optics*. Vol. 3. Englewood Cliffs: Prentice-Hall, 2007.
7. "Cage Systems." *Thorlabs*. N.p., n.d. Web. 20 Mar. 2014. <http://www.thorlabs.us/navigation.cfm?guide_id=2002>.